

## Microfluidic Synthesis

## Novel Application of Polymer Networks Carrying Tertiary Amines as a Catalyst Inside Microflow Reactors Used for Knoevenagel Reactions

Patrik Berg,<sup>[a]</sup> Franziska Obst,<sup>[b]</sup> David Simon,<sup>[b]</sup> Andreas Richter,<sup>[c]</sup> Dietmar Appelhans,<sup>[b]</sup> and Dirk Kuckling\*<sup>[a]</sup>

**Abstract:** A novel application is described for utilizing hydrogel dots as organocatalyst carriers inside microfluidic reactors. Tertiary amines were covalently immobilized in the hydrogel dots. Due to the diffusion of reactants within the swollen hydrogel dots, the accessible amount of catalysts inside a microfluidic reactor chamber can be increased compared to the accessible amount of surface-bound catalysts. To perform fast *Knoevenagel* reactions, important flow parameters had to be validated to optimize the reactor performance while keeping the dimensions of the reactor chamber constant; e.g. the height of the hydrogel dots had to be adjusted to the invariable dimensions of the reactor chamber, or an adjustment of organocatalysts in the hydrogel dots had to be validated to achieve the highest

conversion rate during a certain residence time. To characterize the conversion, nuclear magnetic resonance (NMR) and UV/Vis-spectroscopy were utilized as an offline and online method, respectively. With suitable hydrogel dots, the influence of different flow parameters (e.g., operating flow rate and reactant concentration) on the selected model reactions in the microfluidic reactor was investigated. Finally, a variety of reactants were screened with the optimized flow parameters. With these results, the turnover frequency was determined for the *Knoevenagel* reactions in a microfluidic reactor, and the results were compared with published data that were determined by other synthetic approaches.

## Introduction

In modern chemistry, microfluidic reactors (MFRs) have become increasingly important. In the past, batch reactors were easier to assemble than flow reactors, but today, with modern technical possibilities, there is more hardware that is commercially available to assemble flow reactor systems. Microfluidic pumps with microstepping motors enable flow rates of less than 5  $\mu\text{L}/\text{min}$  (supplier information). In combination with imprinting methods for polydimethylsiloxane,<sup>[1]</sup> 3D printing<sup>[2]</sup> or high-resolution milling cutter,<sup>[3]</sup> all the necessary components to build MFRs are available.

In general, flow reactors combines the benefits of continuous operation,<sup>[4]</sup> online detection<sup>[5]</sup> and reaction parameter adjustment during synthesis<sup>[6]</sup> to optimize the reactor performance. In smaller scaled flow reactors, i.e., microfluidic reactors, further benefits are observed. This includes excellent heat transfer, laminar flow and good control of reaction conditions (temperature, etc.) and several more, which makes the reactions more economic and safer.<sup>[7]</sup> With the previously discussed benefits, a MFR enables good handling and fast screening of different reactions. Finally, different online detection methods, such as NMR,<sup>[8]</sup> HPLC,<sup>[9]</sup> IR,<sup>[10]</sup> mass spectrometry<sup>[11]</sup> or UV/Vis,<sup>[12]</sup> have been successfully used. In addition, MFRs are safer because only small amounts of chemicals are used, and the in situ use of highly reactive or toxic reagents is easily possible.<sup>[13]</sup> All these benefits are important aspects in modern chemistry because of the ongoing importance of "green chemistry".<sup>[14,15]</sup>

Supported organocatalysts are an important research topic because the catalytic activity of organocatalysts can be combined with the physical properties of carrier material to utilize reusable catalysts,<sup>[16,17]</sup> increase catalytic activity<sup>[17]</sup> or long-term use.<sup>[18]</sup> Therefore, this principle is often applied in flow reactors. Already in the 1970s, a fully automated reactor setup was described that used organocatalysts inside a MFR.<sup>[19]</sup> A surface-modified alumina bed was used as a carrier for organocatalysts inside the reactor chamber.

Since the 2000s numerous reactions were performed under flow conditions including the prominent *Knoevenagel* reaction.

[a] P. Berg, Prof. Dr. D. Kuckling  
Department of Chemistry, Faculty of Science, Paderborn University  
Warburger Str. 100, 33098 Paderborn, Germany  
E-mail: dirk.kuckling@uni-paderborn.de  
<https://chemie.uni-paderborn.de/arbeitskreise/organische-chemie/kuckling>

[b] F. Obst, Dr. D. Simon, Dr. D. Appelhans  
Leibniz Institute for Polymer Research Dresden  
Hohe Str. 6, 01069 Dresden, Germany

[c] Prof. Dr. A. Richter  
Institute of Semiconductors and Microsystems, Technische Universität  
Dresden  
Helmholtzstr. 10, 01062 Dresden, Germany

Supporting information and ORCID(s) from the author(s) for this article are available on the WWW under <https://doi.org/10.1002/ejoc.202000978>.

© 2020 The Authors. Published by Wiley-VCH GmbH. This is an open access article under the terms of the Creative Commons Attribution License, which permits use, distribution and reproduction in any medium, provided the original work is properly cited.

Here, mostly inorganic-based materials are used as carrier for catalysts.<sup>[20–24]</sup> This approach can easily be used, however, forces an inaccessible volume within the reactor chamber due to the solid carrier material (Figure 1: blue area). To overcome the limitations given by inaccessible volume swollen polymer networks (gels) were used as carriers.<sup>[18,25–27]</sup> In contrast to monoliths, gels result in a sponge-like structure which avoid any inaccessible volume due to the diffusion of reactants inside the gels (Figure 1). Hence, gels are more effective than monoliths.<sup>[18]</sup> By different processes of gel synthesis it is possible to prepare a homogeneous distribution of immobilized catalysts from gel surface to bulk volume.<sup>[28]</sup> This facilitates to perform the reaction at each location with equal effectivity and without any inactive volume within the reactor chamber. However, compared to inorganic-based materials, polymers as carrier were less often used as support material to perform the *Knoevenagel* reaction.<sup>[29,30]</sup>

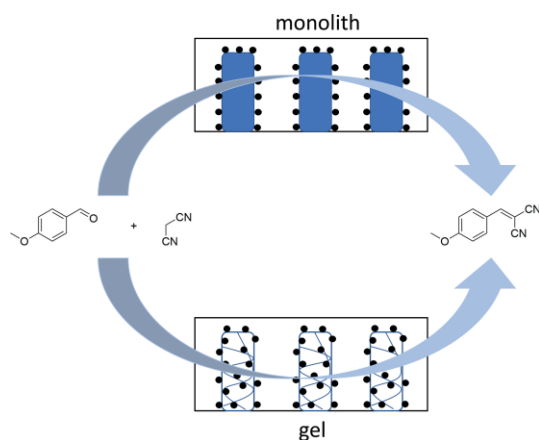


Figure 1. Schematic illustration of monoliths (top way) or gels (bottom way) used as carrier for organocatalysts within reactor chamber and the resulting inaccessible volume (blue) within the reactor chamber (grey box) of each approach.

In general, inorganic materials or polymers as carriers are mostly used within packed-bed flow reactors.<sup>[18,20–23,25–27,29,30]</sup> This type of reactors often uses column-like reactor chambers which require a large amount of catalytically active material<sup>[29,30]</sup> and/or a complex set up with high pressure pumps to enable the flow rate due to the tight packing.<sup>[18,25]</sup> However, high pressure is tough to apply properly due to collapsing and deactivation of poorly cross-linked swollen gels during the flow reaction.<sup>[26]</sup> Beside this poorly cross-linked gels shows weak mechanical stability during processing.<sup>[31]</sup> To face this problem a certain amount of carrier material must be filled into the reactor chamber to be preswollen there.<sup>[18,25,29,30]</sup> It must be mentioned that gels are adaptable structures. Their swelling strongly depends on the surrounding conditions (i.e. solvent). Hence, an important aspect for packed-bed flow reactors is the volumetric limitation of the reactor chamber. If there is a mismatch between the dimensions of the reactor chamber and the volume of isotropically swollen gels, the restriction of the chamber dimensions limits the degree of swelling to a lower level. It is estimated that this forced lower degree of swelling reduces the reactor efficiency.<sup>[26]</sup> It would be expected that the

adjustment of gel size to reactor chamber volume is inevitable to enable highest reactor efficiency.

Micro-structuring of gels via photolithography is a powerful tool to handle this adjustment. This method offers a variety of advantages in contrast to packed-bed flow reactors. For example, with photopatterning the arrangement of the gels could be adjusted by the used masks. As a consequence of the less dense gel structure, and gaps between the gels, a low and controllable backpressure can be realized. Beside this, the size of the gels could be controlled by patterning conditions as well. Due to these facts a MFR was built to utilize gels as carrier for organocatalysts in the *Knoevenagel* reaction in combination with physical advantages of microfluidic set-ups.

Recently, this principle was applied to hydrogel dots with high cross-linker content to be utilized as a cage for enzymes inside microfluidic reactors.<sup>[12]</sup> It was possible to synthesize hydrogel dots with incorporated enzymes via photolithography on glass slides and to successfully use these structures for organic reactions in MFR experiments. Here, diffusion within the hydrogel dots was genetical for performing the reaction. Finally, our approach combines hydrogel dots as a matrix and the immobilization of covalently integrated organocatalysts. This method of integration prevents the bleeding of catalysts. A wide range of low molecular weight catalysts are known that can be applied as monomers.<sup>[32]</sup> Here, the application of hydrogel dots as organocatalyst carrier enables a high variability in the assembled MFR with respect to the performed reaction and the required conditions.

## Results and Discussion

To realize our approach, the assembly of the MFR follows the schematic circuit diagram of Figure 2 A (and Figure S1). Different steps must be accomplished to build the reactor chamber (Figure 2 B and S2).

First, the photopolymerization of the desired ratios of monomers must be optimized (Figure 2 C). In this work, tertiary amines were used to catalyze a number of fast *Knoevenagel* reactions as reported by Diaz.<sup>[16]</sup> These reactions were selected, since the flow rates in the range of  $\mu\text{L}/\text{min}$  and the given volume of reactor chamber restrict the residence time, which can affect the reaction time to the range of a few minutes. For this work, acrylamide compounds were used as catalyst, cross-linker and gel forming agent (Figure 2 C). These monomers were commercially available and provide a good degree of swelling in suitable solvents for the selected *Knoevenagel* reaction. However, the variability of solvents offers a high flexibility of the MFR used for different reactants. Further, the acrylamides enable the fast preparation of the hydrogel dots via photolithography. The resulting hydrogel dots (Figure 2 D) were arranged in a diamond-shaped position for enhancing the residence time of reactants in the reaction chamber. Beside this, this design was selected due to the reduced flow velocity and shear force within the reactor chamber.<sup>[1]</sup> These hydrogel dots were covered with an imprinted PTFE layer (Figure 2 E). This cover layer was imprinted by a high-resolution milling cutter and included a meander-like channel for mixing the reactants because it was

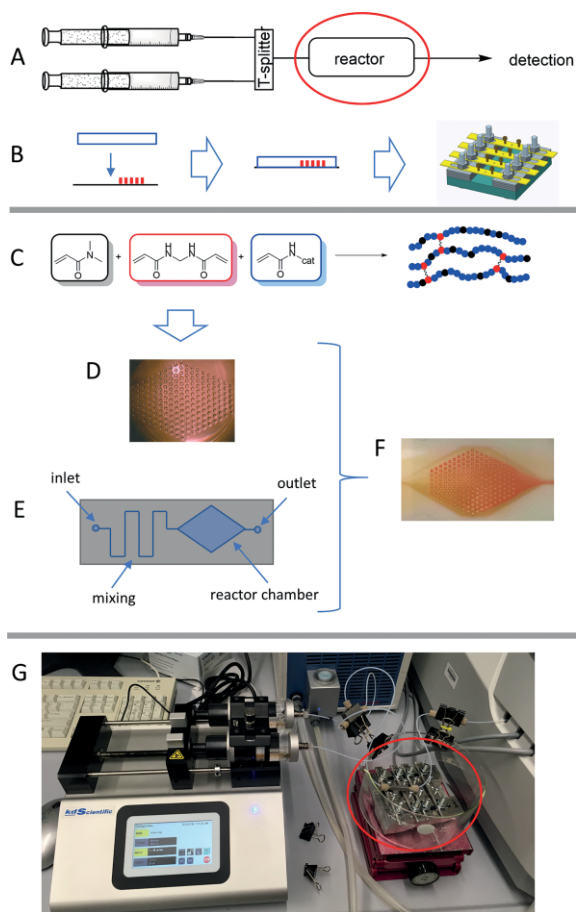


Figure 2. A – Schematic illustration of the MFR system. B – Sequence for assembling the reactor (red circle in A); left – preparation of hydrogel dots on glass surface; middle – covering hydrogel dots with imprinted PTFE cover layer to form reactor chamber; right – alumina frame for fixing and connecting sandwich structure to flow system. C – Structure of the monomers used for the preparation of the hydrogel dots by photolithography; black box = *N,N*-dimethylacrylamide (DMAAm) used for adjusting the catalyst content, red box = methylene(bis)acrylamide (BMA) used as the cross-linker, blue box = *N*-[3-(dimethyl)amino] propylacrylamide (3DMAAAM) as organocatalyst. D – Image of the arranged position of the as-prepared hydrogel dots. E – Schematic illustration of the imprinted structures on the PTFE layer prepared by a high-resolution milling cutter (channel depth of 140  $\mu\text{m}$ ). F – Image of covered hydrogel dots during an MFR experiment. G – Image of the assembled MFR system from the laboratory; the red circle marks the MFR.

shown that this mixer type is most reliable<sup>[33]</sup> as well as the reactor chamber fitting with the diamond shaped position of the hydrogel dots (Figure 2 E). The channels were fabricated with a depth of 140  $\mu\text{m}$ , which yields a reactor chamber volume of 31  $\mu\text{L}$ . Figure 2 F shows the assembled reactor chamber through a transparent bottom of the alumina frame during an experiment. The entire assembled MFR system is shown in Figure 2 G, where the circle indicates the assembled reactor, which is also marked in Figure 2 A.

With this reactor setup, the influence of the different parameters on the reactor conversion was investigated. For example, the influence of the hydrogel dot composition, flow rate or reactant concentration was varied to optimize the reactor performance of the selected *Knoevenagel* reaction. To study the

influences of the different parameters on the *Knoevenagel* reaction, a model system was selected because of the given reactor chamber volume a fast reaction is mandatory.<sup>[16]</sup> For example, it was reported that *p*-anisaldehyde (pAnis) and malononitrile (MDN) can undergo high conversion within 5 min in the presence of a catalyst (Figure 3).<sup>[9]</sup>

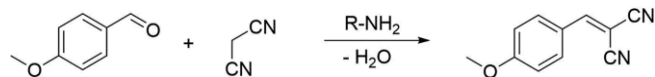


Figure 3. The model reaction of pAnis and MDN as a sample system to indicate reactor efficiency depending on different parameters.

To enable the most efficient use of the reactor chamber, hydrogel dots were used. First, attention must be paid to the physical properties of flexible networks, e.g. the degree of swelling. The reactor itself was assembled by covering the surface-attached hydrogel dots with an imprinted PTFE layer, and everything was fixed in an alumina frame to connect the reactor with the flow system via capillary tubes (Figure 2). The height of the imprinted structures was set to 140  $\mu\text{m}$ . To efficiently use the reactor chamber, it was necessary to adjust the height of the hydrogel dots to the height of the imprinted structures to create structures that completely filled the reactor chamber. The swelling in the *z*-direction of the surface-attached hydrogel dots is calculable from the free swelling results in accordance with R $\ddot{u}$ he.<sup>[34]</sup> Proper polymerization conditions involve the monomer concentration, irradiation time and irradiation intensity. The influence of these parameters on hydrogel dot height was investigated via confocal microscopy (Figure S3–S6). The final polymer preparation was performed with a monomer concentration of 3.7 M, an irradiation time of 9.4 sec and an intensity of 428 mW with an 8 cm distance between the light source and sample. To place the dots properly in the reactor chamber, a suitable mask with a structure of 158 dots in a diamond-shaped position was applied for the imprinted reactor (Figure 2 D).

Full swelling was ensured by using the maximal chamber height, and the degree of swelling of gels had to be determined. Hence, the degree of swelling in water and DMSO depending on the cross-linker content was investigated for the unattached gels within the volume of the samples (equation (1) and Figure S7). Both solvents were suitable for the selected reaction and in agreement with “green chemistry”.<sup>[14,15]</sup> A cross-linker content of 1 mol-% provides the highest degree of swelling and therefore enables the use of an immobilized catalyst in full capacity (Figure S8). Finally, the *Knoevenagel* reaction was carried out in a solvent mixture of 2-propanol/DMSO (1:1) to reduce the surface tension and back pressure of the flow system. From the degree of swelling of the bulk gels in the final solvent mixture, the extension along the *z*-axis of the swollen surface-attached gels depending on the catalyst content could be calculated according to R $\ddot{u}$ he (see SI equation (2)).<sup>[34]</sup> The results are summarized in Table 1. With the calculated *z*-axis degree of swelling, the polymer height in the dry state could be used to adjust the size of hydrogel dots. Therefore, the height of the polymer dots for a polymer composition of 1 mol-% cross-linker and 10, 50 or 90 mol-% catalyst loading was meas-

ured via confocal microscopy (compare Figure S9). Six randomly selected dots on two separately prepared glass slides were measured. To calculate the height in the swollen state, the extension along the z-axis was used in combination with the determined height in the dry state (Figure S10).

As seen from Table 2, hydrogel dots with a catalyst loading of 90 mol-% fit the swollen state to the height of the reactor chamber. Thus, this polymer composition was determined in accordance with reaching the highest conversion of the MFR. To investigate the reactor performance, it was first necessary to determine the conversion of the selected reactions in the absence of a catalyst. This is an important aspect for the offline determination of the conversion, since the reactants are mixed in the inlet and outlet phase and might further react while accumulating. Further, the concentration of the reactants must be optimized to meet the needs of different analysis methods.

The amount of synthesized product was limited in the  $\mu\text{L}/\text{min}$  range by the flow rate and the reactant concentration up to solvent saturation. The results of the blank *Knoevenagel* reaction with different aldehydes and two CH-active compounds (MDN and ethyl cyanoacetate (ECAC)) are summarized in Table S1. For all the reactions, a concentration was used so that the reactants and products were always dissolved. As observed, it is not possible to store the reactants together before the experiment and to collect a product solution over a long period until analysis of conversion is performed due to blank reaction. To directly measure the conversion after the reaction, a continuous analysis via a flow cuvette (size of flow cell 6.2  $\mu\text{L}$ ) was used in combination with UV/Vis spectroscopy. For this method, calibration curves of pure substances must be determined to transform the absorbance into conversion (SI, chapter 2.4). In addition to UV/Vis spectroscopy, it was also possible to determine the conversion in a discontinuous procedure by NMR.

For this method, it was necessary, especially for the MDN, to divide the sample collection into smaller time periods to reduce the influence of the blank conversion on the reactant conversion due to residence time in the collection vessel (see Table S1). Hence, the samples were collected over 1 h and then were

frozen immediately to stop the reaction. The samples were warmed just before measuring the NMR spectra.

With the model reaction of pAnis and MDN (Figure 3), the MFR experiments were performed to compare both the detection methods. Figure 4 shows a similar behavior of the conversion vs. time curves for the shape of curves, maximum conversion and long-term conversion ( $\geq 25$  h) of the continuous and discontinuous detection methods. From Figure 4, a decrease in the reactor conversion was observed. This effect can also be tracked visually by the appearance of the gel dots. Due to the transparent bottom of the MFR, the dots inside the reactor chamber could be observed. The reaction of 3,5-dichloro-2-hydroxybenzaldehyde and MDN was selected due to their highest reaction rates of all the performed *Knoevenagel* reactions (see Table S1). The product of this reaction has a pink color, which indicates conversion inside the MFR chamber (Figure 5). During the 8 h experiment, the color of the gel dots changed

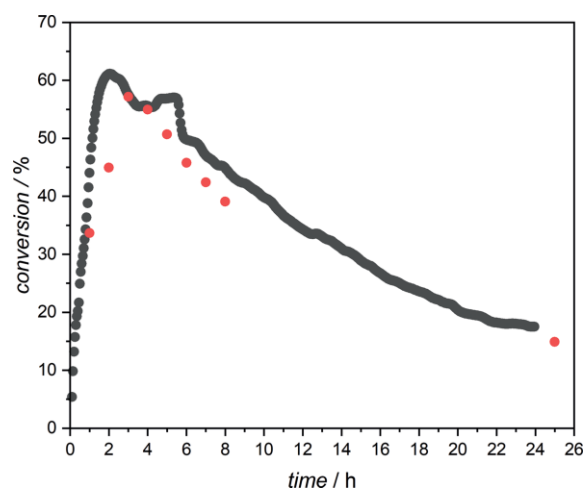


Figure 4. Comparison of conversion-time-diagram of the continuous (black dots) analysis via UV/Vis spectroscopy and the discontinuous (red dots) analysis via NMR spectroscopy of the model reaction with pAnis and MDN (1 M each) under an operating flow of 2  $\mu\text{L}/\text{min}$  and a polymer composition of 90 mol-% catalyst, 9 mol-% DMAAm and 1 mol-% BMA.

Table 1. Degree of swelling in 2-propanol/DMSO (1:1) for unattached polymers with 1 mol-% cross-linker content and calculated z-axis degree of swelling for attached polymers.

Catalyst loading [mol-%] <sup>[a]</sup>	Degree of swelling [-] unattached polymer networks	Calculated extension along z-axis [-] attached hydrogel dots
10	8.6 ( $\pm 0.6$ )	3.3
50	7.9 ( $\pm 0.7$ )	3.2
90	7.0 ( $\pm 1.1$ )	2.9

[a] Polymers prepared from a total monomer concentration of 3.7 M with 428 mW UV-light intensity and 1 mol-% cross linker, differences were adjusted with *N,N*-dimethylacrylamide.

Table 2. Determined height of hydrogel dots in a dried state and the calculated height in swollen state by approximation.

Catalyst loading [mol-%] <sup>[a]</sup>	Height of dry state [ $\mu\text{m}$ ]	Calculated height of swollen state [ $\mu\text{m}$ ]	Filling of reactor chamber [%] <sup>[b]</sup>
10	32 ( $\pm 2.9$ )	109	80
50	40 ( $\pm 2.2$ )	128	90
90	44 ( $\pm 4.7$ )	130	90

[a] Polymers were prepared from total monomer concentration of 3.7 M with 428 mW UV-light intensity and 1 mol-% cross linker, differences were adjusted with *N,N*-dimethylacrylamide. [b] Calculated with the set height of imprinted structures of 140  $\mu\text{m}$ .



from colorless to brown, which is assumed to be due to the enrichment of MDN (the MDN that was purchased from the supplier was brown colored) and product within the dots.

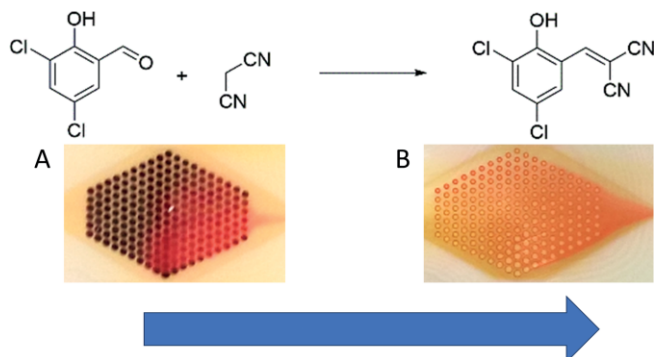


Figure 5. Images of polymer gel dots during the MFR reaction of 3,5-dichloro-2-hydroxybenzaldehyde with MDN after A - 1 h and B - 8 h by using a polymer composition of 90 mol-% 3DMAPAAm, 9 mol-% DMAAm and 1 mol-% BMA. The flow direction is from left to right along the blue arrow.

The diffusion of the reactants into the hydrogel dots and the reactions occurring inside the dots influence the efficiency of the hydrogel dots in a complex manner, e.g. degree of swelling and chemical composition. When this MFR experiment was repeated, comparable results were observed with respect to the average conversion and the shape of the conversion-time diagram (Figure S13). For four different MFR experiments, an average conversion of 55 ( $\pm 7$ ) % over the first 8 h was calculated. This result shows that this system is robust against external influences during the assembly or running process.

In general, the online detection (UV/Vis) of the reactor performance is most beneficial for a continuous flow reactor because of the ability to make feasible online adjustments to optimize reactor performance. However, NMR is the most suitable method to analyze the reaction mixture with respect to all the included compounds (e.g., reactants, products, and side reactions).

An important parameter of the flow system was the catalyst loading of the hydrogel dots. To identify the best catalyst loading, flow experiments were performed with 0, 10, 50 and 90 mol-% catalyst-loaded hydrogel dots, and the results were analyzed with NMR (Figure 6) for the model reaction (Figure 3). From the NMR spectra, the average conversion was calculated during the 1 h time periods (Figure S14).

Without a catalyst, only a small amount of product was detected as shown in Table S1, while an increase in the product concentration was observed for catalyst loading from 10 to 50 mol-%. In contrast, at 90 mol-% catalyst loading, the conversion leveled off, and a similar behavior was determined for catalyst loading at 50 mol-% (Table 3). The two curves show only a small difference in the product concentration during the first 8 h. However, the long-term activity (more than 25 h) revealed a product concentration of 0.05 M for 90 mol-% catalyst loading and 0.01 M for 50 mol-% catalyst loading (Figure S15). Hence, the best polymer network composition was 90 mol-% catalyst, 9 mol-% DMAAm and 1 mol-% BMA because after a running time of > 22 h, 50 mol-% catalyst loading produces only slightly more product than the catalyst loading of 0 and 10 mol-% (Fig-

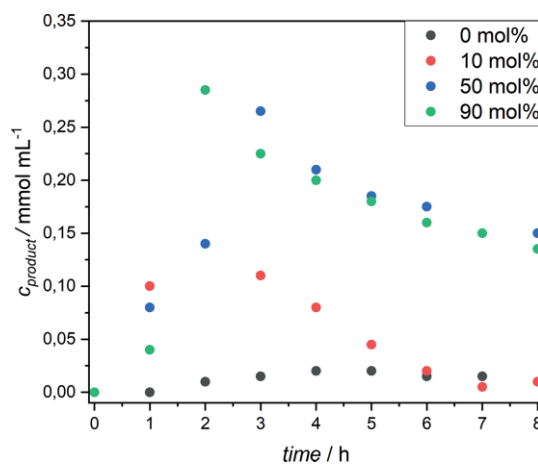


Figure 6. Reactor conversion vs. running time as determined via NMR for the model reaction of pAnis and MDN (1 M) and polymer samples with 0 (black dots), 10 (red dots), 50 (green dots) and 90 mol-% (blue dots) catalyst loading and 1 mol-% BMA with a flow rate of 2  $\mu\text{L}/\text{min}$ . Data of 10 and 50 mol-% at 2 h, 50 and 90 mol-% at 7 h, as well as 0 and 10 mol-% at 8 h overlaps at the same value.

ure S15). The similar effectivity of 50 and 90 mol-% during first 8 h running time can be explained by the weak dependence of gel composition and degree of swelling. Thereby, a catalysts content of 90 mol-% within the gel forces a higher reactant conversion in comparison to catalysts content of 50 mol-% due to the equally swollen state of gels at each composition. It is assumed that in case of other monomers showing a stronger dependence of gel composition and degree of swelling the most beneficial composition must be found and will be an equilibrium between the catalytic activity of the gel and the swelling behavior.

Table 3. Average conversion of the model reaction of pAnis and MDN (1 M each) after 8 h with a flow rate of 2  $\mu\text{L}/\text{min}$ . Bracketed values describes the highest determined conversion during 8 h MFR running time.

catalyst loading [mol-%]	0	10	50	90
average conversion [%]	2 (4)	10 (28)	30 (53)	31 (57)

Following these results, the reactant concentration in the MFR was varied to characterize the MFR efficiency. Different concentrations of starting material, up to the saturation of MDN (in a 2 M stock solution) for the model reaction (Figure 3), were tested.

Figure 7 (A) shows an increase in the reactor efficiency depending on the concentration following the second-order kinetics of the model reaction. This behavior is also indicated by the exponential slope shown in Figure 7 (B). The results shown in Figure 7 show that the best MFR performance was reached with a 2 M reactant concentration. The last parameter considered to influence the MFR performance was the flow rate. The standard conditions with an operating flow rate of 2.0  $\mu\text{L}/\text{min}$  were compared with flow rates of 4.0 and 8.0  $\mu\text{L}/\text{min}$ . Table 4 lists the residence times inside the reactor chamber and the average conversion of the model reaction (Figure 3) with a concentration of 2 M. An increasing flow rate resulted in a decrease in the conversion in the reactor chamber (Table 4). This increase in flow rate is responsible for the reduced residence time inside

the reactor chamber. Thus, the most beneficial flow rate was 2  $\mu\text{L}/\text{min}$ . In Table 4, the highest total amount of product generated within 8 h was obtained for a flow rate of 8  $\mu\text{L}/\text{min}$ . However, it was generated with a four times higher amount of reactant (from 0.96 mmol for 2  $\mu\text{L}/\text{min}$  to 3.84 mmol for 8  $\mu\text{L}/\text{min}$ ) that was pumped through the reactor by using a reactant stock solution of 2 M.

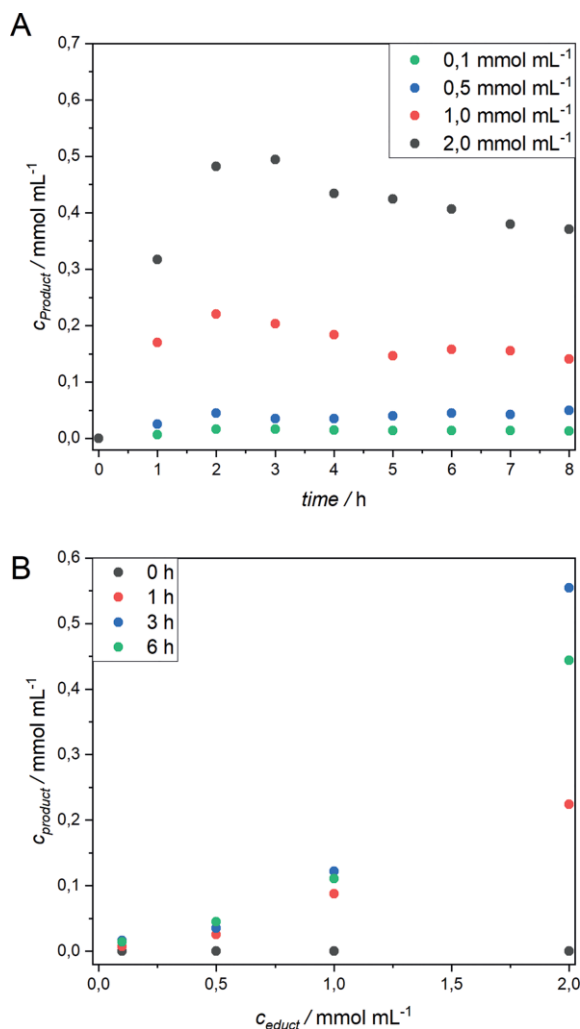


Figure 7. A – Screening of the reactor efficiency for the model reaction (Figure 3) depending on the reactant concentration at 0.1 (blue dots), 0.5 (green dots), 1.0 (red dots) and 2.0 M (black dots) reactant stock solution via <sup>1</sup>H-NMR spectroscopy. B – Product concentration depending on the reactant concentration in the MFR for 0 h (black dots), 1 h (red dots), 3 h (green dots) and 6 h (blue dots) with the running time detected via NMR using a gel composition of 90 mol-% catalyst and 1 mol-% cross-linker at a flow rate of 2.0  $\mu\text{L}/\text{min}$ .

Table 4. The average conversion for the model reaction of pAnis and MDN (2 M) depending on the operating flow rate and residence time inside the MFR chamber.

Flow rate [ $\mu\text{L}/\text{min}$ ]	Residence time [min] <sup>[a]</sup>	Average conversion [%] <sup>[b]</sup>	Product [mmol] <sup>[c]</sup>
2.0	18	44	0.42
4.0	9	19	0.36
8.0	5	12	0.46

[a] Residence time calculated with a MFR chamber volume of 31  $\mu\text{L}$ . [b] Polymer composition of 90 mol-% catalyst, 1 mol-% cross linker and 9 mol-% DMAAm, prepared from 3.7 M monomer concentration. [c] Calculated from the reactant concentration which is pumped through the reactor chamber over 8 h.

These results show that a high flow rate is not economical due to the high amount of unreacted compounds. A reduction in flow rate to less than 2  $\mu\text{L}/\text{min}$  was also not useful due to the crystallization of reactants from the reaction mixture at the outlet capillary tube. This crystallization is caused by the evaporation of volatile solvents, resulting in a blocking of the MFR. A closer look at the conversion-time diagrams of the model reaction for the different flow rates (Figure 8) revealed that the conversion decreased more rapidly with increasing flow rate. Under a higher flow rate, a higher amount of reactants were pumped through the reactor in a certain time, and there was less time remaining for the diffusion of reactants within the dots. With the results shown in Figure 6, Figure 7, and Figure 8, the best polymer network composition, reactant concentration and flow rate were found. With these parameters, a reactant screening was performed (Figure S16–S22). Therefore, two reference measurements were done. First, the flow experiment was compared with a reference experiment under beneficial flow conditions by using hydrogel dots without a catalyst (composition of 99 mol-% DMAAm and 1 mol-% BMA). Second, the flow experiment was compared with a batch experiment, in which an equal amount of low molecular weight catalyst (3DMAAm) and residence time was applied. Thus, it was necessary to calculate the amount of catalyst inside the 158 gel dots. With the height and diameter, which was determined by confocal microscopy, the volume of the dried hydrogel dots was calculated (Figure S9). The mass of hydrogel dots was calculated via the

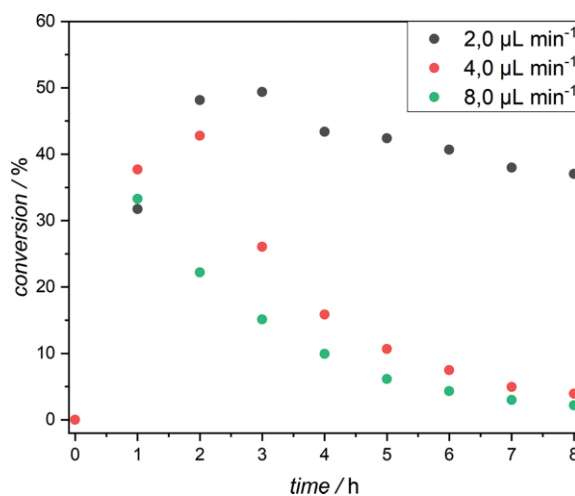


Figure 8. Conversion-time-diagram of the model reaction between pAnis and MDN (2 M) with polymer dots prepared from 90 mol-% catalyst-loading and 1 mol-% cross-linker. The different flow rates were screened at 2.0  $\mu\text{L}/\text{min}$  (black dots), 4.0  $\mu\text{L}/\text{min}$  (red dots) and 8  $\mu\text{L}/\text{min}$  (green dots).

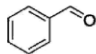
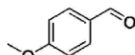
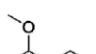
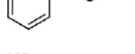
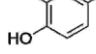
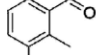
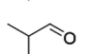
density that was identified for the hydrogels (0.90 ( $\pm 0.06$ ) g/mL), which is in accordance with the literature for DMAAm gels.<sup>[35]</sup> The maximum mass of hydrogel dots was determined from the total irradiated volume of the 3.7 M monomer mixture in a certain composition and correlates to a 45 % yield. With this result, the amount of catalyst inside the attached hydrogel dots (with composition of 90 mol-% 3DMAPAAm, 9 mol-% DMAAm and 1 mol-% BMA) was 2.2  $\mu$ mol for a reactor chamber of 31  $\mu$ L and 158 dots. With an operating flow rate of 2.0  $\mu$ L/min, a 0.96 mL of reactant solution was pumped through the reactor for 8 h. This indicates that 2.2  $\mu$ mol catalyst was used for the 0.96 mL of reactant mixture. This was a catalyst content of approximately 0.25 mol-% with respect to reactants. This batch reaction was run for 15 min, corresponding to the residence time of the reactant mixture inside the reactor chamber with an operating flowrate of 2.0  $\mu$ L/min.

The comparison of the flow experiment with the catalyst and the batch reference values showed that the flow experiment could be more effective (Table 5, reactions 2, 4, 5, and 6). An advantage of flow reactors is the continuous synthesis of products. It was observed that 2.2  $\mu$ mol catalyst can be used for over 6 d for a *Knoevenagel* reaction. For the reaction of pAnis and MDN, an average conversion of approximately 25 % was observed (Figure S23). Here, in total, 16.8 mL of reactant solution was pumped through the reactor chamber. For a comparable batch reaction, a reactant solution with as low as 0.01 mol-% of catalyst with respect to reactants must be used. It was also shown that an almost constant conversion could be ob-

tained for 5–6 d, indicating that the running time of the reactor can be prolonged to more than 6 d without a further decrease in conversion. Comparable results for the reaction of pAnis and ECAC were observed (Figure S23).

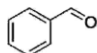
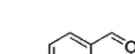
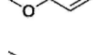
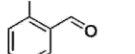
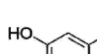
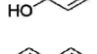
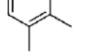
ECAC was used in addition to MDN as a CH-active compound. With ECAC, a more complex product structure was created, in particular, *E/Z* isomers of the product. In addition, a long-term experiment was also performed (Figure S23). The same conversion behavior was observed for pAnis and MDN. ECAC is less active than MDN, which results in a lower conversion (compare Table S1). Hence, it was possible to determine the reactor conversion with only one averaged <sup>1</sup>H-NMR sample. The results are summarized in Table 6. Lower conversions were obtained as found for the reaction of MDN with different aldehydes (Table 5), which can undoubtedly be explained by reactant reactivity (Table S1). Nevertheless, there was almost no conversion obtained under batch conditions. Furthermore, *E/Z*-ratios of almost 100:0 were determined for the conversion of ECAC due to steric hindrance between ester functions and aromatic or aliphatic residues, and these results were in accordance with literature reports.<sup>[16]</sup> To compare the MFR efficiency with other

Table 5. MFR conversions for different aldehyde reactants with MDN.

Reaction	Aldehyde <sup>[a]</sup>	Flow experiment [%] <sup>[b]</sup>	Reference flow experiment [%] <sup>[b,c]</sup>	Batch reference [%] <sup>[b,d]</sup>
1		27	5	43
2		44	3	16
3		32	1	39
4		22	1	9
5		41	7	38
6		29	0	24
7		25	0	49

[a] Aldehyde and MDN stock solution concentration = 2 M. [b] Calculated from <sup>1</sup>H-NMR spectra of reaction solution in respect to aldehyde. [c] Reference was measured with a gel composition of 99 mol-% DMAAm and 1 mol-% cross-linker. [d] Batch conditions were 0.25 mol-% of low molecular weight catalyst and reaction time of 15 min.

Table 6. MFR conversion of different aldehyde reactants with ECAC.

Reaction	Aldehyde <sup>[a]</sup>	Flow experiment [%] <sup>[b,c]</sup>	Reference flow experiment [%] <sup>[b,d]</sup>	Batch reference [%] <sup>[b,e]</sup>
1		20 (100/0)	0	2
2		24 (100/0) <sup>[f]</sup>	0	0
3		24 (100/0)	0	1
4		5 (100/0)	0	0
5		29 (100/0)	0	0
6		21 (100/0)	0	0
7		17 (100/0)	0	2

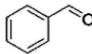
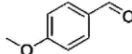
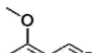
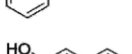
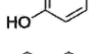
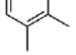
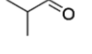
[a] Aldehyde and MDN stock solution concentration = 2 M. [b] Calculated from <sup>1</sup>H-NMR spectra of the reaction solution in respect to aldehyde. [c] Bracketed values describe the *E/Z* ratio. [d] Reference values were measured with a gel composition of 99 mol-% DMAAm and 1 mol-% cross-linker. [e] Batch conditions were 0.25 mol-% of low molecular weight catalyst and a reaction time of 15 min. [f] The configuration was confirmed via the characteristic *trans*-CN–H coupling constant of reference substances.

approaches, the turnover frequency of the catalyst was calculated. The respected values are summarized in Table 6.

Several different catalysts used in batch reactions were described for the reaction of benzaldehyde with MDN. According to the literature, immobilized primary amines enable TOF from  $50 \text{ h}^{-1}$ <sup>[36]</sup> up to  $577 \text{ h}^{-1}$ .<sup>[37]</sup> However, these values are hardly comparable, since the TOF depends on reactants and on reaction parameters.

Therefore, TOFs were calculated for similar systems as reported by Diaz.<sup>[16]</sup> 4-methoxybenzaldehyde and malononitrile reach a TOF of  $44 \text{ h}^{-1}$  and an ECAC of  $20 \text{ h}^{-1}$ . In comparison with the results summarized in Table 7, the catalysts reported in the literature were two times more active. These differences can be explained by the catalyst activity, with the primary amines being more active than the tertiary amines. Another example using tertiary amines shows that the reaction of pAnis with MDN or ECAC could be performed with a high yield and a TOF of  $7 \text{ h}^{-1}$ .<sup>[38]</sup> This result shows that the reported MFR is more active. Tertiary amines applied in our approach are two times more active for the reaction of pAnis with ECAC and three times more active for the reaction with MDN than these same reactions in a comparable system.

Table 7. Calculated TOF of different reactions. TOF was calculated in respect to a residence time of 15 min. Here,  $2.2 \times 10^{-3} \text{ mmol}$  of catalyst (immobilized on surface), a 1 M reactant solution and the average conversion over 8 h running time of the MFR were used for calculations.

Reaction	Aldehyde <sup>[a]</sup>	TOF of reaction with MDN [ $\text{h}^{-1}$ ]	TOF of reaction with ECAC [ $\text{h}^{-1}$ ]
1		15	11
2		24	13
3		17	13
4		12	3
5		22	16
6		16	11
7		14	9

## Conclusion

The successful use of hydrogel dots as carriers for organocatalysts within a microfluidic reactor was described. Initially, the height of the hydrogel dots was adjusted with respect to catalyst loading. Therefore, the proper conditions for the initial photopolymerization were found. The conditions were used to adjust the height in the dry state because the height in the swol-

len state was estimated by relation from the literature. The immobilized catalyst was used for a *Knoevenagel* reaction. Here, the flow parameters for this type of reaction were modified to optimize the reactor performance. To analyze the reactor performance two different methods were established. It was shown that an online detection (UV/Vis) and offline method (NMR) could be used comparably. Additionally, this method was observed to be robust against external influences, such as differences during the assembly or operation process. By using the NMR detection method, influences on the reactor conversion were investigated by changing generic parameters, such as flow rate, concentration and catalyst loading. With the optimized parameters, the MFR was successfully used for screening different reactants. Here, the steric claim of the substituents and the reactant reactivity (MDN and ECAC) were changed. The screening of different reactants was compared with a reference flow reaction (without catalysts) and with a comparable batch reaction. Here, it was seen that the benefits of flow reactors do not clearly occur for each example of highly reactive reactants. However, for the less reactive reactions, the MFR was several times more effective than a comparable batch reaction. By using ECAC as the reactant, the *E/Z* ratio was also investigated. Here, it was observed that the results were in accordance with those in the literature. The described system can be used for long-term experiments (over 140 h). The conversion-time diagram shows a plateau of conversion, which indicates that an increase in the MFR time can be expanded without any restrictions.

## Experimental Section

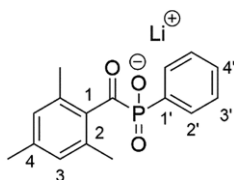
**Chemicals:** The monomers *N,N*-dimethylacrylamide (> 99 %) (DMAAm) and *N*-[3-(dimethylamino)propyl]acrylamide (98 %) (3DMAPAAm) were purchased from Tokyo Chemical Industries (TCI). The cross-linker *N,N*-bismethylacrylamide (99+ %) were purchased from Acros Organics. The reactants for initiator synthesis, dimethylphenylphosphonite (98 %) was purchased from Sigma-Aldrich, while 2,4,6-trimethylbenzoylchlorid (98+ %) and 2-butanon (99 %) were purchased from Alfa Aesar. 3-(trichlorosilyl)propylmethacrylate (> 90 %) used for surface modification and was purchased from Sigma-Aldrich. The used solvents for flow experiments, dimethyl sulfoxide (DMSO) analytical grade, and isopropanol (technical grade) were purchased from Grüssing GmbH. The polydimethylsiloxane (PDMS), to fabricate the imprinted PDMS layer, was purchased from VWR ("Sylgard® 184 Siliconelastomer Kit"). For flow reactions different aldehydes and  $\beta$ -dicarbonyl compounds were used. Malononitrile (99 %) was purchased from Janssen Chemica and cyanoacetic acid ethyl ester (98 %) was purchased from Ferak. Benzaldehyde (98 %) was purchased from TCI and isovaleraldehyde (97 %), isobutyraldehyde (98 %), 4-methoxybenzaldehyde (98 %) were purchased from Sigma Aldrich. The substituted benzaldehydes, 2-methoxybenzaldehyde (98 %), 2-hydroxy-3-methoxybenzaldehyde (96 %), 3,4-dihydroxybenzaldehyde (97 %) and 2-hydroxy-3,5-dichlorobenzaldehyde (98 %) were purchased from Lancaster. 2,3-dimethylbenzaldehyde (97 %) was purchased from Alfa Aesar.

**Analysis Methods:** The confocal microscope Keyence "VK-9700" was used for height determination of polymer dots. Images were taken with the software "VK Viewer 2.4.0.1" and the analysis of polymer height was done with the software "VK Analyzer 3.4.0.1". The



$^1\text{H-NMR}$  spectra for conversion determination were measured on a Bruker "Avance 300" spectrometer. Product spectra of synthesised products were measured on a Bruker "Avance 500" spectrometer for  $^1\text{H}$ -,  $^{13}\text{C}$ - and  $^{31}\text{P}$ -NMR spectra. UV/Vis spectra were measured with a "Specord50plus" photometer, from Jena Analytik. For time dependent conversion measurements, the kinetic program of "ASpectUV 1.2.3" software was used in combination with a flow through cuvette, from HellmaAnalytics, with 6.2  $\mu\text{L}$  flow cell volume. The ESI-MS measurements were done with a "Synapt-G2 HDMS" mass spectrometer, from Waters. The spectrometer is used in combination with a time-of-flight analyser.

**Initiator Synthesis:** The initiator synthesis was done according to Majima et al.<sup>[39]</sup> Under argon atmosphere dimethylphenylphosphonite (1.6 mL, 1.56 g, 11.3 mmol) was put inside a 50 mL round-bottomed flask. 2,4,6-trimethyl-benzoyl chloride (1.5 mL, 1.65 g, 9.0 mmol) was added dropwise by a dropping funnel. After complete addition the reaction was stirred 24 h in darkness at room temperature. Then potassium bromide (3.2 g), dissolved in 2-butanone (50 mL), were added. The mixture was heated to 50  $^\circ\text{C}$  for 10 min, and then stirred for further 4 h in darkness at room temperature. The formed solid was filtered by Büchner funnel and washed two times with 2-butanone (100 mL). The final product was isolated with 66 % yield.



$^1\text{H-NMR}$  in  $\text{D}_2\text{O}$  (500 MHz):  $\delta$  (ppm) = 2.01 (6H; 2- $\text{CH}_3$ ; s); 2.16 (3H; 4- $\text{CH}_3$ ; s); 6.80 (2H; 3; s); 7.42 (2H; 3'; dt ( $^3J_{\text{HH}} = 7.7$  Hz,  $^3J_{\text{HH}} = 3.1$  Hz)); 7.49 (1H; 4'; t ( $^3J_{\text{HH}} = 7.8$  Hz)); 7.73 (2H; 2'; dd ( $^3J_{\text{HH}} = 7.3$  Hz;  $^3J_{\text{HH}} = 11.4$  Hz));  $^{13}\text{C-NMR}$  in  $\text{D}_2\text{O}$  (125 MHz):  $\delta$  (ppm) = 18.7 (2- $\text{CH}_3$ ); 20.3 (4- $\text{CH}_3$ ); 128.1 (CH-4'); 128.4/128.5 (CH-3'); 132.1 (CH-3); 132.3/132.4 (CH-2'); 132.5 (C-1'); 133.5 (C-4); 133.7 (C-1); 138.0/138.3 (C-2); 238.8 (1-CO);  $^{31}\text{P-NMR}$  in  $\text{D}_2\text{O}$  (202 MHz):  $\delta$  (ppm) = 12.31 (s); ESI-MS;  $m/z$  (relative intensity): Calculated for  $[\text{C}_{16}\text{O}_3\text{PH}_{16}\text{Li} + \text{H}]^+$  295.1070 found 295.1055 (75 %); Calculated for  $[\text{C}_{16}\text{O}_3\text{PH}_{16}\text{Na} + \text{H}]^+$  311.0808 found 311.0795 (100 %); Calculated for  $[\text{C}_{16}\text{O}_3\text{PH}_{16}\text{Li} + \text{Na}]^+$  317.0889 found 317.0880 (25 %).

**General Procedure for Reaction Under Batch Conditions:** 2 mL of aldehyde (2 M) in 2-propanol/DMSO (v:v = 1:1) stock solution was mixed with desired ration (0.25 or 5 mol-%) of catalyst. Afterwards, 2 mL of malononitrile (2 M) or ethyl cyanoacetate (2 M) in 2-propanol/DMSO (v:v = 1:1) stock solution were added. The mixture was stirred at room temperature for 8 h. For high active malononitrile each hour 100  $\mu\text{L}$  sample for NMR measurement was taken, while reaction with ECAc a sample after 8 h was taken. For purification the reaction mixture was mixed with 10 mL of water. The suspension was stirred with 70 mL of diethyl ether for at least 4 h. The organic phase was isolated by filtration through a phase separation filter (Macherey-Nagel "MN 617 WA"). The solvent was evaporated, and the product was dried in vacuo.

**Surface Modification:** The polymers were bound to glass slides (7.6 cm  $\times$  2.6 cm), purchased from Carl Roth. The microscope slides were washed with 2-propanol under supersonic treatment at 70  $^\circ\text{C}$  for 10 min. Afterwards, also under supersonic treatment at 70  $^\circ\text{C}$ , the microscopy slides were cleaned with water and at last with ethanol. After drying in nitrogen flow these substrates were modified by gas deposition. 20 of the dried slides were placed in a desic-

cator with 300  $\mu\text{L}$  of 3-(trichlorosilyl)propylmethacrylate with 50 mbar vacuum for at least 2 h. A successful modification could be proofed by the hydrophobic effect of glass surface.

**Photopolymerization:** The photopolymerization is carried out via an "Omnicure<sup>®</sup> S1500" UV-Lamp, from Lumen Dynamics. UV irradiation for photopolymerization was done with an intensity of 428 mW (intensity = 20 %) at the end of the lighting cable, with 8 cm distance of light source to substrate. 15 mmol of monomers were mixed in the desired ratios and were dissolved in 1.7 mL of deionized water with an initiator concentration of 17.5 mg/mL. 195  $\mu\text{L}$  of monomer solution were put into an incubation chamber gasket, from ThermoFisher. The incubation chamber gasket was covered by a modified microscopy slide and the photopolymerization mask (diamond shaped position of 158 dots) on the back side. This sandwich was centered below UV light for 9.4 s. Afterwards the incubation chamber was removed, and the polymer structures were washed in 2-propanol for 18 h. The substrate with polymer dots were dried in air and stored at room temperature.

**Reactor Set Up:** The flow system was set up according to the following schematic illustration (Figure S1). The flow rate was generated by a "Legato 200" syringe pump, from KDSscientific. As reservoirs two "Hamilton 1000 series" syringes were used. All tubes are PTFE capillary tubes with iD = 0.2 mm, from Fisher Scientific. The reactor itself is a self-made alumina holder (Figure S2) to connect imprinted PDMS or PTFE layer with the flow system. The reactor design is described by Simon et al.<sup>[12]</sup> Polymer dots on microscopy slides were inserted into the reactor by covering the polymer structure with an imprinted PDMS or PTFE layer. The channel height on these imprinted covers were approximately 140  $\mu\text{m}$ . This sandwich was inserted into the alumina holder (Figure S2) and fixed by screws with torque of 8 cN/m. The PDMS or PTFE layer could be connected to the alumina holder with special screw threads and drill holes to capillary tubes.

**Flow Reaction:** First the polymer dots were pre-swollen with 2-propanol/DMSO (v:v = 1:1) mixture for at least 2 h. Therefore, the "Legato 200 Syringe" pump was loaded with two syringes (Braun 20 mL syringe with iD = 20.1 mm), filled up with pure solvent mixture and the flow rate were set to 4.0  $\mu\text{L}/\text{min}$ . Afterwards the syringe pump was loaded with reactant syringes (Hamilton 1000 series). Flow rate was set on 2.0  $\mu\text{L}/\text{min}$ . Finally, the conversion of resulting product was determined.

**Determination of Conversion:** The conversion was determined by NMR spectroscopy or UV/Vis spectroscopy. NMR spectroscopy enables an offline determination of conversion and a fast screening of different reactions, while UV/Vis enables an online determination with very high sensitivity during the whole reactor run. For NMR spectroscopy the outlet flow was collected into a vial with 400  $\mu\text{L}$   $[\text{D}_6]\text{DMSO}$  and was frozen immediately after 1 h of sample collection with liquid nitrogen. The sample was warmed up just before the tube is inserted into the NMR spectrometer.

**Determination of Degree of Swelling:** The degree of swelling was determined by measuring length and diameter of prepared polymer samples. Therefore, 0.5 mL of the monomer mixture in desired ration (see chapter 1.5 – Photopolymerization) was inserted into 1 mL plastic-pipette. The solution was irradiated with UV-light for 9.4 sec with an intensity of 40 % (compare chapter 1.5 – Photopolymerization). Afterwards, the plastic-pipette was cut into pieces to extract the cylindrical polymer gel. For 1 day a lixiviation with isopropanol was done, before the sample was cut into smaller pieces. At the end the samples were dried at 50  $^\circ\text{C}$  for several day until a constant mass was observed. With light microscope the length and

diameter of the samples were measured by a microscopic ruler. Following, the samples were swollen in the desired solvent overnight. In the end the sample were also measured with microscopic ruler.

With the volume in dry and swollen state the degree of swelling was calculated after following equation (1):

$$d = \frac{V_{\text{swollen}}}{V_{\text{dry}}} \quad (1)$$

d	Degree of swelling [-]
$V_{\text{swollen}}$	Volume of swollen gel [mm <sup>3</sup> ]
$V_{\text{dry}}$	Volume of dry gel [mm <sup>3</sup> ]

## Acknowledgments

We acknowledge the Paderborn University Faculty of Engineering for providing the confocal microscope. Open access funding enabled and organized by Projekt DEAL.

**Keywords:** Microfluidic reactor · Hydrogel dots · Immobilized organocatalysts · Organocatalytic reaction · Green chemistry

- [1] F. Obst, D. Simon, P. J. Mehner, J. W. Neubauer, A. Beck, O. Stroyuk, A. Richter, B. Voit, D. Appelhans, *Beilstein J. Org. Chem.* **2019**, *31*, 9684.
- [2] C. M. B. Ho, S. H. Ng, K. H. H. Li, Y.-J. Yoon, *Lab on a Chip* **2015**, *15*, 3627.
- [3] D. J. Guckenberger, T. E. de Groot, A. M. D. Wan, D. J. Beebe, E. W. K. Young, *Lab on a chip* **2015**, *15*, 2364.
- [4] G. Jas, A. Kirschning, *Chem. Eur. J.* **2003**, *9*, 5708.
- [5] C. J. Welch, X. Gong, J. Cuff, S. Dolman, J. Nyrop, F. Lin, H. Rogers, *Org. Process Res. Dev.* **2009**, *13*, 1022.
- [6] D. C. Fabry, E. Sugiono, M. Rueping, *React. Chem. Eng.* **2016**, *1*, 129.
- [7] a) X. Yao, Y. Zhang, L. Du, J. Liu, J. Yao, *Renewable Sustainable Energy Rev.* **2015**, *47*, 519; b) K. S. Elvira, X. Casadevall I Solvas, R. C. R. Wootton, A. J. deMello, *Nat. Chem.* **2013**, *5*, 905; c) J. Wegner, S. Ceylan, A. Kirschning, *Chem. Commun.* **2011**, *47*, 4583; d) V. Hessel, H. Löwe, *Chem. Eng. Technol.* **2005**, *28*, 267; e) K. Jähnisch, V. Hessel, H. Löwe, M. Baerns, *Angew. Chem. Int. Ed.* **2004**, *43*, 406; *Angew. Chem.* **2004**, *116*, 410; f) G. Vesper, *Chem. Eng. Sci.* **2001**, *56*, 1265.
- [8] D. A. Foley, E. Bez, A. Codina, K. L. Colson, M. Fey, R. Krull, D. Piroli, M. T. Zell, B. L. Marquez, *Anal. Chem.* **2014**, *86*, 12008.
- [9] J. P. McMullen, M. T. Stone, S. L. Buchwald, K. F. Jensen, *Angew. Chem. Int. Ed.* **2010**, *49*, 7076; *Angew. Chem.* **2010**, *122*, 7230.
- [10] J. S. Moore, K. F. Jensen, *Org. Process Res. Dev.* **2012**, *16*, 1409.
- [11] B. P. Loren, M. Wlekinski, A. Koswara, K. Yammine, Y. Hu, Z. K. Nagy, D. H. Thompson, R. G. Cooks, *Chem. Sci.* **2017**, *50*, 10083.
- [12] D. Simon, F. Obst, S. Haefner, T. Heroldt, M. Peiter, F. Simon, A. Richter, B. Voit, D. Appelhans, *React. Chem. Eng.* **2019**, *4*, 67.
- [13] a) M. O'Brien, I. R. Baxendale, S. V. Ley, *Org. Lett.* **2010**, *12*, 1596; b) C. B. McPake, C. B. Murray, G. Sandford, *Tetrahedron Lett.* **2009**, *50*, 1674.
- [14] J. H. Clark, *Green Chem.* **1999**, *1*, 1.
- [15] P. T. Anastas, J. C. Warner, *Green chemistry. Theory and practice*, Oxford Univ. Press, Oxford, **2000**.
- [16] D. Kühbeck, G. Saidulu, K. R. Reddy, D. D. Díaz, *Green Chem.* **2012**, *14*, 378.
- [17] H. A. Zayas, A. Lu, D. Valade, F. Amir, Z. Jia, R. K. O'Reilly, M. J. Monteiro, *ACS Macro Lett.* **2013**, *2*, 327.
- [18] P. Llanes, C. Rodríguez-Escrich, S. Sayalero, M. A. Pericas, *Org. Lett.* **2016**, *18*, 6292.
- [19] R. W. Coughlin, M. Aizawa, B. F. Alexander, M. Charles, *Biotechnol. Bioeng.* **1975**, *17*, 515.
- [20] S. M. Lai, C. P. Ng, R. Martin-Aranda, K. L. Yeung, *Microporous Mesoporous Mater.* **2003**, *66*, 239.
- [21] P. Watts, C. Wiles, *Chem. Eng. Technol.* **2007**, *30*, 329.
- [22] C. Wiles, P. Watts, S. J. Haswell, *Tetrahedron* **2004**, *60*, 8421.
- [23] G. Zhang, T. Zhang, X. Zhang, K. L. Yeung, *Catal. Commun.* **2015**, *68*, 93.
- [24] X. Zhang, E. S. Man Lai, R. Martin-Aranda, K. L. Yeung, *Appl. Catal. A* **2004**, *261*, 109.
- [25] S. B. Ötvös, I. M. Mándity, F. Fülöp, *J. Catal.* **2012**, *295*, 179.
- [26] X. C. Cambeiro, R. Martín-Rapún, P. O. Miranda, S. Sayalero, E. Alza, P. Llanes, M. A. Pericàs, *Beilstein J. Org. Chem.* **2011**, *7*, 1486.
- [27] M. Planchestainer, M. L. Contente, J. Cassidy, F. Molinari, L. Tamborini, F. Paradisi, *Green Chem.* **2017**, *19*, 372.
- [28] a) M. Benaglia, A. Puglisi, F. Cozzi, *Chem. Rev.* **2003**, *103*, 3401; b) J. Lu, P. H. Toy, *Chem. Rev.* **2009**, *109*, 815.
- [29] H. Ishitani, Y. Saito, Y. Nakamura, W.-J. Yoo, S. Kobayashi, *Asian J. Org. Chem.* **2018**, *7*, 2061.
- [30] D.-Z. Xu, S. Shi, Y. Wang, *RSC Adv.* **2013**, *3*, 23075.
- [31] K. Haraguchi, H.-J. Li, *Macromolecules* **2006**, *39*, 1898.
- [32] a) X. Yu, A. Herberg, D. Kuckling, *Eur. Polym. J.* **2019**, *120*, 109207; b) P. Riente, J. Yadav, M. A. Pericàs, *Org. Lett.* **2012**, *14*, 3668; c) T. E. Kristensen, T. Hansen, *Eur. J. Org. Chem.* **2010**, *2010*, 3179.
- [33] P. J. Mehner, F. Obst, D. Simon, J. Tang, A. Beck, D. Gruner, M. Busek, D. Appelhans, U. Marschner, B. Voit et al. in *Print Proceeding of the ASME Convergence on Smart Materials, Adaptive Structures and Intelligent Systems, Volume 1: Development and Characterization of Multifunctional Materials* (Ed.: The American Society of Mechanical Engineers (ASME)).
- [34] R. Toomey, D. Freidank, J. Rühle, *Macromolecules* **2004**, *37*, 882.
- [35] J. Chen, H. Park, K. Park, *J. Biomed. Mater. Res.* **1999**, *44*, 53.
- [36] Y. Luan, Y. Qi, H. Gao, R. S. Andriamitantoa, N. Zheng, G. Wang, *J. Mater. Chem. A* **2015**, *3*, 17320.
- [37] K. Isobe, T. Hoshi, T. Suzuki, H. Hagiwara, *Mol. Diversity* **2005**, *9*, 317.
- [38] G. Li, J. Xiao, W. Zhang, *Green Chem.* **2011**, *13*, 1828.
- [39] T. Majima, W. Schnabel, W. Weber, *Makromol. Chem.* **1991**, *192*, 2307.

Received: July 15, 2020